Supplemental material for: Hole spin resonance and spin-orbit coupling in a silicon metal-oxide-semiconductor field-effect transistor

K. Ono[1*†],G. Giavaras[2†], T. Tanamoto[3], T. Ohguro[3], X. Hu[2,4], and F. Nori[2,5]
[1]*Advanced device laboratory, RIKEN, Wako-shi, Saitama 351-0198, Japan*
[2]*CEMS, RIKEN, Wako-shi, Saitama 351-0198, Japan*
[3]*Corporate R&D Center, Toshiba Corporation, Kawasaki-shi, Kanagawa 212-8582, Japan*
[4]*Department of Physics, University at Buffalo, SUNY, Buffalo, New York 14260-1500, USA and*
[5]*Department of Physics, The University of Michigan, Ann Arbor, MI 48109-1040, USA*

I. DOUBLE QUANTUM DOT: COULOMB DIAMOND AND CURRENT

Most of the features of the open Coulomb diamond structure shown in Fig. 1(c) in the main article can be well reproduced by a simple calculation based on the constant charging-energy model. If N_i ($i = 1, 2$) is the number of holes on dot i, then the energy of dot 1 is $E_1(N_1, N_2) = E_{C1}N_1 + E_{C12}N_2 - C_1V_G - D_1V_S + E_{\rm off}$, and the energy of dot 2 is $E_2(N_1, N_2) = E_{C12}N_1 + E_{C2}N_2 - C_2V_G - D_2V_S$. Here, E_{Ci} ($i = 1, 2$) and E_{C12} denote an on-site and an inter-dot charging energy respectively. Also, C_i and D_i are the lever arms of V_G and V_S, while $E_{\rm off}$ is the energy offset between the dots. The Coulomb blockade is lifted for $eV_S > E_1(N_1+1, N_2) > E_1(N_1, N_2+1) > 0(= eV_D)$. Figure S1 shows a typical Coulomb diamond structure for a double quantum dot when one of the dots has large charging energy, and the other dot has small charging energy.

In Fig. 1(c) in the main article, a region where spin blockade occurs was identified. The transport cycle in the spin blockade regime is shown schematically in Fig. S2. As explained in the main article the spin-orbit interaction and the microwave field can lift the spin blockade by inducing singlet-triplet transitions. As a result a measurable leakage current flows through the double quantum dot. Figure S3 shows the intensity plot of the leakage current I_D for the same scale of magnetic field B and MW frequency f as that in Fig. 1(e) in the main article (where dI_D/dB was presented). The high-current curves are due to microwave-induced transitions between the mixed singlet-triplet states. The series of resonances at constant MW frequency are due to photon-assisted tunneling enhanced by cavity modes.

II. SPIN RESONANCE FOR LARGE MAGNETIC FIELD

In the main article we presented EDSR spectra near the T_+–S anti-crossing point [Fig. 1(e)]. Here we show additional spectra for a microwave frequency up to 40 GHz and magnetic field up to 1.7 T. In Fig. S4 three nearly-straight lines are visible. As explained in the main article, two of these lines map-out the transitions between the states $T_\pm$ and S. The lower line corresponds to the 2-photon T_+–S transition. For a double quantum dot with large difference in the g-factors, the lines $T_\pm$–S are not parallel at high magnetic fields. Investigation of the data shown in Fig. S4 demonstrates that in our system these lines are parallel within at least 2% accuracy, indicating that the g-factor difference in the two dots is small enough compared with the zero-field singlet-triplet splitting of about 5 GHz.

III. MICROWAVE ATTENUATION AND NONLINEARITY

In this section we present some details about the microwave field. If we assume a 50 Ohm impedance for our transmission line, then the MW power (in dBm) used in the experiment [Fig. 2(a) and Fig. 3(a, c, e)], and the corresponding MW amplitude (in mV) are:
-40 dBm 2.2 mV,
-30 dBm 7.1 mV,
-22 dBm 17.8 mV,

* E-mail address: k-ono@riken.jp
† these authors contributed equally to this work

-20 dBm 22.4 mV.
For the calculations [Fig. 2(b) and Fig. 3(b, d, f)] we have the following correspondence:
-87 dBm 0.01 mV,
-67 dBm 0.1 mV,
-61 dBm 0.2 mV,
-55 dBm 0.4 mV.

The experimental and theoretical numbers are quite different, suggesting a very large attenuation and nonlinearity. An estimated attenuation of our rigid coaxial cable with a 2 m length is only 3 dB at 5 GHz. This very large attenuation and nonlinearity may be due to the bare wiring of about 1 cm length between the end of the coax and our device, as well as the nonlinearity of the capacitance. Our MOSFET device is set around the subthreshold regime, thus the capacitance will be affected by the voltages V_S, V_G as well as the MW power, if a strong power starts to cause photon-assisted tunneling or charge pumping current.

Moreover, from the geometry of our device we expect that the microwave field which is applied to the top gate modulates to some degree the energies of both quantum dots. However, to obtain the EDSR signal we have to consider a time-dependent energy detuning, i.e., a time-dependent energy difference between the dot energies. In contrast to our MOSFET device, in standard gate-defined quantum dots the microwave field is typically applied to an independent local gate defining one of the two dots, so a time-dependent energy detuning can be produced without significant attenuation. This fact seems to support the relatively strong MW power considered in our experiment.

In Fig. 1(e) in the main article we presented EDSR spectra for the voltages $V_S = 25$ mV and $V_G = 0.597$ V. In Fig. S5(a) we present results for fixed $V_S = 25$ mV and three different values of V_G. As can be seen, tuning V_G leads to different EDSR peak positions, which can be attributed to a different singlet-triplet energy splitting due to a change in the energy detuning. Here, the (average) g-factor of the double dot does not show any noticeable change with V_G. Figure S5(b) shows the V_G dependence of the EDSR peak position at fixed $B = 100$ mT. The slope near $V_G = -560$ mV is about 0.2 GHz/mV, but the observed nonlinearity is important and has to be considered especially for large MW amplitudes, such as 20 mV. This observation could be one of the sources of the discrepancy between the theoretical and experimental numbers given above for the MW powers and amplitudes.

IV. SYSTEM HAMILTONIAN

In this section we describe the Hamiltonian of the physical system. We consider a double quantum dot (DQD) coupled to metallic leads. The total Hamiltonian of the system is

$$H = H_{\rm DQD} + H_{\rm L} + H_{\rm T}, \tag{1}$$

where $H_{\rm DQD}$ is the DQD Hamiltonian, $H_{\rm L}$ is the Hamiltonian of the leads, and $H_{\rm T}$ is the interaction Hamiltonian between the DQD and the leads. Specifically, the DQD Hamiltonian is

$$H_{\rm DQD} = \sum_{i=1}^{2} \left(\varepsilon_i n_i + U_i n_{i\uparrow} n_{i\downarrow} - \frac{1}{2} g_i \mu_B B (n_{i\uparrow} - n_{i\downarrow}) \right) + H_{\rm c} + H_{\rm so}, \tag{2}$$

where n_i is the number operator $n_i = \sum_\sigma n_{i\sigma} = c^\dagger_{i\uparrow} c_{i\uparrow} + c^\dagger_{i\downarrow} c_{i\downarrow}$, and the operator $c^\dagger_{i\sigma}$ ($c_{i\sigma}$) creates (destroys) a hole on dot $i = 1, 2$, with spin $\sigma = \{\uparrow, \downarrow\}$ and orbital energy ε_i. We assume a single-band description and consider the holes to have spin 1/2. In this case the two-hole Hilbert space is spanned by the singlet and triplet states $|T_\pm\rangle$, $|T_0\rangle$, $|S_{11}\rangle$, $|S_{20}\rangle$, $|S_{02}\rangle$, where $|S_{km}\rangle$ is a singlet state with k (m) holes on dot 1 (dot 2). A similar approach was employed by Zarassi *et al* in Ref. [1] to explore the magnetic field evolution of the spin blockade in Ge/Si nanowires. In our study we do not identify the heavy- and light-hole compositions. Generally, in an acceptor and/or a quantum dot the electronic states are mixtures of spin as well as heavy- and light-hole bands, and are split by the quantum confinement. The observed EDSR spectra should contain contributions from both heavy- and light-hole components. Here, we simply take advantage of the fact that without any strict selection rule, the EDSR transitions between the lowest Kramers pair of states in the acceptor/dot are allowed. The theoretical results suggest that considering only spin-1/2 holes in the dynamics is sufficient to reproduce the basic experimental observations.

The orbital energies of the two dots are

$$\varepsilon_1 = \frac{\delta}{2}, \qquad \varepsilon_2 = -U_2 - \frac{\delta}{2} + A\cos(\omega t), \tag{3}$$

where δ denotes the energy detuning. The external electric field has amplitude A and cyclic frequency $\omega = 2\pi f$, and when $A \neq 0$ the DQD Hamiltonian is time dependent $H_{\rm DQD} = H_{\rm DQD}(t)$. This configuration of the orbital energies results in a localised spin in dot 2 during the transport cycle in the spin blockade regime.

Each dot has a charging energy U_i, and g-factor g_i which leads to a Zeeman splitting $g_i\mu_{\rm B}B$ due to the external magnetic field B. The inter-dot tunnel coupling with strength $t_{\rm c}$ is modelled by the Hamiltonian

$$H_{\rm c} = -t_{\rm c}\sum_{\sigma} c^{\dagger}_{1\sigma}c_{2\sigma} + \text{H.c.}, \tag{4}$$

and the non spin-conserving inter-dot tunnel coupling due to the spin-orbit interaction (SOI) is modelled by the Hamiltonian [2, 3]

$$H_{\rm so} = -t_{\rm so}\sum_{\sigma\sigma'} c^{\dagger}_{1\sigma}(i\sigma^{y})_{\sigma\sigma'}c_{2\sigma'} + \text{H.c.}. \tag{5}$$

This simplified Hamiltonian couples $|S_{02}\rangle$ ($|S_{20}\rangle$) to $|T_{\pm}\rangle$ states, thus for example the lowest singlet-triplet levels anti-cross and the induced gap is proportional to the SOI tunnel coupling $t_{\rm so}$. For a fixed $t_{\rm so}$ the anti-crossing gap is sensitive to the detuning δ because this controls the amplitude of the $|S_{02}\rangle$ component in the quantum states. A rigorous derivation of a microscopic SOI Hamiltonian [4] should consider the detailed geometry of the quantum dot system which in the present device is unknown. Furthermore, to simplify the analysis we assume that the microwave field affects only the energy of dot 2, while all the other DQD parameters remain fixed. This basic assumption gives a very good qualitatively agreement with the experiment.

The DQD is tunnel-coupled to left and right leads, which consist of non-interacting holes. These holes are described by the Hamiltonian

$$H_{\rm L} = \sum_{\ell k\sigma} \epsilon_{\ell k} d^{\dagger}_{\ell k\sigma} d_{\ell k\sigma}, \tag{6}$$

where the operator $d^{\dagger}_{\ell k\sigma}$ ($d_{\ell k\sigma}$) creates (destroys) a hole in lead $\ell = \{L, R\}$ with momentum k, spin σ, and energy $\epsilon_{\ell k}$. The interaction Hamiltonian between the DQD and the two leads is

$$H_{\rm T} = \sum_{k\sigma}(t_L c^{\dagger}_{1\sigma}d_{Lk\sigma} + t_R c^{\dagger}_{2\sigma}d_{Rk\sigma}) + \text{H.c.}, \tag{7}$$

with t_L (t_R) being the tunnel coupling between dot 1 (2) and the left (right) lead, which is assumed to be energy independent, and we also consider $t_L = t_R$.

V. TWO-LEVEL MODEL

A. Two-level Hamiltonian

In the main article an effective two-level Hamiltonian was used to explore the microwave-induced peaks. Here we give some details about the derivation of this Hamiltonian. First we diagonalize the time-independent part of the DQD Hamiltonian $H_{\rm DQD}$. The derived eigenenergies are denoted by E_i and the corresponding eigenstates are written in the general form

$$|u_i\rangle = a_i|S_{11}\rangle + b_i|T_{+}\rangle + c_i|S_{02}\rangle + d_i|T_{-}\rangle + e_i|T_0\rangle. \tag{8}$$

For only one state the coefficient $e_i \neq 0$ and specifically $e_i = 1$, and for simplicity we neglect the component $|S_{20}\rangle$, but this is taken into account in the numerical computations. Then we write the total DQD Hamiltonian $H_{\rm DQD}$ in the energy basis $|u_i\rangle$. To look for an analytical treatment, we assume that the two eigenstates $|u_1\rangle$, $|u_2\rangle$, which form the anti-crossing point, can approximate well the dynamics of the system and thus we ignore all the other eigenstates. These arguments lead to the following approximate DQD Hamiltonian

$$h^{'}_{\rm DQD} = \begin{pmatrix} E_1 & 0 \\ 0 & E_2 \end{pmatrix} + A\cos(\omega t)\begin{pmatrix} 1+c_1^2 & c_1c_2 \\ c_1c_2 & 1+c_2^2 \end{pmatrix}, \tag{9}$$

where E_1, E_2 are the two energy levels which anti-cross. Then to remove the time dependence from the diagonal elements of $h^{'}_{\rm DQD}$, we perform a transformation to derive the transformed Hamiltonian [5]

$$h_{\rm DQD} = U^{\dagger}(t)h^{'}_{\rm DQD}U(t) - i\hbar U^{\dagger}(t)\frac{dU(t)}{dt}, \tag{10}$$

with the operator

$$U(t) = \begin{pmatrix} e^{i\phi_1(t)} & 0 \\ 0 & e^{i\phi_2(t)} \end{pmatrix}, \tag{11}$$

and the phases

$$\phi_{1,2}(t) = -\frac{(1+c_{1,2}^2)A}{\hbar\omega}\sin(\omega t) \pm \frac{n\omega t}{2}. \tag{12}$$

The transformed Hamiltonian is

$$h_{\mathrm{DQD}} = \begin{pmatrix} E_1 + n\hbar\omega/2 & q \\ q^* & E_2 - n\hbar\omega/2 \end{pmatrix}, \tag{13}$$

with the off-diagonal coupling element being

$$q = \frac{c_1 c_2 A}{2}\left[\exp(+i\omega t) + \exp(-i\omega t)\right]\exp(-in\omega t)\exp\left(i\frac{\Lambda}{\hbar\omega}\sin(\omega t)\right), \tag{14}$$

and the parameter $\Lambda = A(c_1^2 - c_2^2)$. To simplify this expression we use the formula

$$\exp[ix\sin(\omega t)] = \sum_m \exp(im\omega t) J_m(x), \tag{15}$$

where J_m is the mth order Bessel function of the first kind. Then the coupling term is

$$q = \frac{c_1 c_2 A}{2}\sum_m \exp[i(m-n+1)\omega t] J_m\left(\frac{\Lambda}{\hbar\omega}\right) + \frac{c_1 c_2 A}{2}\sum_m \exp[i(m-n-1)\omega t] J_m\left(\frac{\Lambda}{\hbar\omega}\right). \tag{16}$$

In the context of a 'rotating wave approximation', we assume that in the long-time limit, when the system has reached the steady state, the non-oscillatory terms can approximate well the dynamics. Thus, the off-diagonal element becomes time-independent

$$q \approx \frac{c_1 c_2 A}{2} J_{n-1}\left(\frac{\Lambda}{\hbar\omega}\right) + \frac{c_1 c_2 A}{2} J_{n+1}\left(\frac{\Lambda}{\hbar\omega}\right). \tag{17}$$

Using the property $xJ_{n-1}(x) + xJ_{n+1}(x) = 2nJ_n(x)$ and substituting $\Lambda = A(c_1^2 - c_2^2)$, we arrive at the off-diagonal coupling element

$$q = n\hbar\omega \frac{c_1 c_2}{c_1^2 - c_2^2} J_n\left(\frac{A(c_1^2 - c_2^2)}{\hbar\omega}\right), \quad n = 1, 2, ... \tag{18}$$

We use the effective DQD Hamiltonian h_{DQD} to study the n-photon resonance that satisfies the condition $n\hbar\omega = E_2 - E_1$. For $n = 1$, the Hamiltonian h_{DQD} coincides with the Hamiltonian in Eq. (1) given in the main article. Because the Hamiltonian h_{DQD} that describes the n-photon transition depends on n, in Figs. 3(b, d, f) in the main article we consider $1 \leq n \leq 4$, and for each frequency of the driving field we plot the corresponding maximum increase in the background current that comes from a specific n. This way produces the correct behaviour near the n-photon peak.

When there is no driving, $A = 0$, the coupling is $q = 0$; thus the two levels are uncoupled and there are no microwave-induced peaks. Moreover, when $t_{\mathrm{so}} = 0$ one of the coefficients c_i is zero; thus $q = 0$ and the driving field cannot couple the two levels. Finally, the parameters in this work satisfy the regime $J_1(x) > J_n(x)$ with $n > 1$, consequently at a given magnetic field the single-photon peak is stronger than the n-photon peak. This observation is consistent with the experimental data.

B. Rate equations

In the spin blockade regime the electrical transport takes place through the charge-cycle $(0,1) \to (1,1) \to (0,2) \to (0,1)$, where $(k,\ m)$ refers to a state with k (m) holes on dot 1 (dot 2). We consider the single-spin states $c_{2\uparrow}^\dagger|0\rangle$,

$c^\dagger_{2\downarrow}|0\rangle$, as well as the two-hole states that form the anti-crossing $|u_1\rangle$, $|u_2\rangle$, and determine the density matrix $\rho(t)$ of the DQD in the transformed frame ('rotating' frame). Following a standard open-system approach [6] the equation of motion of $\rho(t)$ can be written in the form

$$\frac{d\rho(t)}{dt} = -\frac{i}{\hbar}[h_{\rm DQD}, \rho(t)] + \mathcal{L}\rho(t), \tag{19}$$

where the incoherent term $\mathcal{L}\rho(t)$ accounts for the interaction of the DQD with the two leads which is treated to second order in the dot-lead tunnel coupling (sequential tunneling). In this approximation the transition rates between the DQD eigenstates due to the coupling of the DQD with the leads acquire a simple form [3]. The effect of the transformation $U(t)$ on the DQD-lead interaction is ignored and Eq. (19) can be solved analytically in the steady state, e.g., when $d\rho(t)/dt = 0$. In this effective model the electrical current through the DQD is proportional to the population of the $|S_{02}\rangle$ state, which is extracted directly from the populations of $|u_1\rangle$ and $|u_2\rangle$.

VI. FLOQUET MODEL

The effective two-level model described in the preceding section takes into account only the states which form the anti-crossing point and neglects the time-dependent oscillating terms in the Hamiltonian. In the charge-cycle in the spin blockade regime all triplet states are relevant [3], and in the limit $B \to 0$ the triplet states become quasi degenerate, thus the effective model is questionable. Therefore, to test the overall accuracy of the effective model, we describe in this section another model that takes into account all the states which are involved in the transport through the DQD [7], and treats the time dependence of the DQD Hamiltonian $H_{\rm DQD}(t)$ exactly within the Floquet formalism [8–10].

A. Floquet Hamiltonian

The Hamiltonian of the DQD is periodic $H_{\rm DQD}(t) = H_{\rm DQD}(t+T)$, with $T = 2\pi/\omega$ being the period of the external electric field. For this reason it is convenient to apply the Floquet formalism which is a powerful tool for time-dependent periodic systems [8–10]. According to the Floquet theorem, a solution of the time-dependent Schrödinger equation with a periodic Hamiltonian can be written in the form

$$|\psi_j(t)\rangle = \exp\left(-i\frac{\epsilon_j t}{\hbar}\right)|\phi_j(t)\rangle, \tag{20}$$

where $|\phi_j(t)\rangle$ are the Floquet modes which have the periodicity of the Hamiltonian, i.e., $|\phi_j(t)\rangle = |\phi_j(t+T)\rangle$, and ϵ_j are the Floquet energies. These are time independent and can be defined, for instance, within the interval $-\hbar\omega/2 < \epsilon_j < +\hbar\omega/2$. The Floquet modes and energies satisfy the following eigenvalue problem [11]

$$\left(H_{\rm DQD}(t) - i\hbar\frac{\partial}{\partial t}\right)|\phi_j(t)\rangle = \epsilon_j|\phi_j(t)\rangle, \tag{21}$$

that is solved by expanding the time periodic $H_{\rm DQD}(t)$ and $|\phi_j(t)\rangle$ in a Fourier series:

$$[H_{\rm DQD}(t)]_{nm} = \sum_k e^{ik\omega t}[H^k_{\rm DQD}]_{nm}, \quad |\phi_j(t)\rangle = \sum_k e^{ik\omega t}|\phi^k_j\rangle. \tag{22}$$

If we denote by $|y_i\rangle$ the basis vectors spanning the DQD Hilbert space, and expand $|\phi^k_j\rangle$ in that basis

$$|\phi^k_j\rangle = \sum_{i=1}^{\mathcal{N}} W^k_{i,j}|y_i\rangle, \tag{23}$$

the eigenvalue problem Eq. (21) becomes

$$\sum_{l=1}^{\mathcal{N}}\sum_k \left([H^{n-k}_{\rm DQD}]_{il} + n\hbar\omega\delta_{nk}\delta_{il}\right)W^k_{l,j} = \epsilon_j W^n_{i,j}. \tag{24}$$

Here the indexes n, k refer to the Fourier series, and the indexes i, l refer to the basis vectors. For the numerical computations, this infinite system of coupled equations is truncated to a finite but sufficiently large value to ensure good convergence of the results.

B. Master equation

In the Floquet formalism, the density matrix $\rho(t)$ of the DQD is expressed in the time-dependent Floquet basis $|\phi_j(t)\rangle$, simplifying drastically the calculation of the steady state [8–10]. Within the Born and Markov approximations, the matrix elements $\rho_{ij}(t)$ satisfy the master equation

$$-\left(\frac{\partial}{\partial t}+\frac{i}{\hbar}\epsilon_{ij}\right)\rho_{ij}(t)=\sum_{kl}\rho_{lj}(t)X_{ik;lk}(t)+\rho_{ik}(t)G_{lj;lk}(t)-\rho_{kl}(t)[G_{ik;jl}(t)+X_{lj;ki}(t)]. \tag{25}$$

with $\epsilon_{ij}=\epsilon_i-\epsilon_j$, and the transition rates $X(t)$ and $G(t)$ quantify the interaction of the DQD with the two leads. For simplicity, here we focus only on $X(t)$ and consider only the interaction of dot 1 with the left lead. The coupling of the DQD to the right lead can be treated in a similar manner. The rate $X_{ij;kl}(t)$ is defined by the Fourier expansion

$$X_{ij;kl}(t)=\sum_K e^{iK\omega t}X_{ij;kl}(K), \tag{26}$$

$$\begin{aligned}X_{ij;kl}(K)=&\Gamma\sum_{M\sigma}[c_{1\sigma}(K+M)]_{ij}[c_{1\sigma}(M)]^*_{kl}f_L(\epsilon_{lk}-M\hbar\omega)\\&+\Gamma\sum_{M\sigma}[c_{1\sigma}(-K-M)]^*_{ji}[c_{1\sigma}(-M)]_{lk}f_L^-(\epsilon_{kl}+M\hbar\omega),\end{aligned} \tag{27}$$

where f_L is the Fermi distribution at the chemical potential of the left lead and $f_L^-=1-f_L$. The subband index is defined by the index M. The DQD-lead coupling constant Γ is proportional to t_L^2, and the matrix element is defined through its Fourier transform as follows

$$[c_{1\sigma}(M)]_{ij}=\frac{1}{T}\int_0^T e^{-iM\omega t}\langle\phi_i(t)|c_{1\sigma}|\phi_j(t)\rangle dt. \tag{28}$$

For any two system operators s_p and s_w, with $s_p^\dagger=s_w$, the corresponding matrix elements satisfy $[s_p(-M)]^*_{ji}=[s_w(M)]_{ij}$. To solve Eq. (25) we assume that in the long-time limit the density matrix, which describes the steady state, has the same periodicity as the DQD Hamiltonian, thus it can be expressed in the form

$$\rho_{ij}(t)=\sum_N e^{iN\omega t}\rho_{ij}(N). \tag{29}$$

Substituting Eq. (26) and Eq. (29) into Eq. (25) results in an infinite set of coupled equations that is solved numerically by truncating N to a finite value. Having determined the steady state, the tunneling current is computed by taking the average of the current operator $I=ei[H,N_R]/\hbar$, where $N_R=\sum_{k\sigma}d^\dagger_{Rk\sigma}d_{Rk\sigma}$ is the number of holes in the right lead. In the presence of the microwave field the time-averaged current is computed.

Figure S6 shows the background current and the microwave-induced peak height near the T_+–S anti-crossing point for a microwave amplitude $A=30$ μeV. The basic features are in good overall agreement with the experimental data [see main article Fig. 2(c) and (d)]. The height of the current peaks is sensitive to the DQD-lead coupling Γ and the microwave amplitude A. When Γ is strong, A has to be large for the peaks to be visible. However, the computational time increases quickly with A, because the Fourier expansions need extra terms to converge. For this reason, to keep the numerical problem tractable we choose Γ in the GHz range.

A more detailed fit to the background current can be achieved by coupling the DQD to a bosonic bath and introducing spin flips [12, 13]. This approach offers limited additional insight into the present experimental data, whilst extra parameters have to be introduced to specify the spectral density of the bath. Therefore, this approach is not pursued in this work. Three-body states which for simplicity are not accounted for in our model can also have some contribution to the background current [13].

Finally, we mention that the Floquet model can also be used to assess the rotating wave approximation [Eqs. (16), (17)] in the effective two-level model. In this case the Hamiltonian $H_{\rm DQD}(t)$ in Eq. (21) has to be replaced by $h'_{\rm DQD}(t)$ [Eq. (9)]. The two models are in agreement.

VII. DOUBLE QUANTUM DOT PARAMETERS

The experimental data suggests that the charging energies of the two dots are $U_1\approx 25$ meV and $U_2\approx 5$ meV and the g-factor is $g\approx 1.8$ (see main article). In the calculations we take for the two dots $g_1=g_2$, though this assumption

is not important for the theoretical results presented in this work. In the experiment an anti-crossing point is probed at about 200 mT and the anti-crossing gap is about 1 GHz, but the exact values of the parameters δ, t_c, and t_{so} are unknown. Consequently, for the calculations we choose δ, t_c, and t_{so} in order to form an anti-crossing point as in the experiment, and simultaneously to achieve a good qualitative agreement between the calculated and the measured background currents ($A = 0$). The SOI Hamiltonian H_{so} forms two anti-crossing points, but the observed spectra indicate that only one point is relevant for the chosen ranges of the magnetic field and the driving frequency. The choice of the parameters δ, t_c, and t_{so} is not unique and we choose different values in the two models in order to achieve a good fit to the background current. In the two-level model, the parameters are $\delta = -1.85$ meV, $t_c = 0.135$ meV, and $t_{so} = 0.15t_c$; and in the Floquet model the parameters are $\delta = -1.98$ meV, $t_c = 0.14$ meV, and $t_{so} = 0.14t_c$. Here, we present results for $\delta < 0$, but the models can also produce the general experimental features for $\delta > 0$.

[1] A. Zarassi, Z. Su, J. Danon, J. Schwenderling, M. Hocevar, B. M. Nguyen, J. Yoo, S. A. Dayeh, and S. M. Frolov, Phys. Rev. B **95**, 155416 (2017).
[2] J. Stehlik, M. Z. Maialle, M. H. Degani, and J. R. Petta, Phys. Rev. B **94**, 075307 (2016).
[3] G. Giavaras, N. Lambert, and F. Nori, Phys. Rev. B **87**, 115416 (2013).
[4] V. N. Golovach, A. Khaetskii, and D. Loss, Phys. Rev. B **77**, 045328 (2008).
[5] M. Grifoni and P. Hänggi, Phys. Rep. **304**, 229 (1998).
[6] K. Blum, *Density Matrix Theory and Applications* (Springer, Berlin, 2012).
[7] We neglect three-body states and consider in total 11 many-body states.
[8] G. Platero and R. Aguado, Phys. Rep. **395**, 1 (2004).
[9] S. I. Chu and D. A. Telnov, Phys. Rep. **390**, 1 (2004).
[10] S. Kohler, J. Lehmann, and P. Hanggi, Phys. Rep. **406**, 379 (2005).
[11] P. Brune, C. Bruder, and H. Schoeller, Phys. Rev. B **56**, 4730 (1997).
[12] S. Chorley, G. Giavaras, J. Wabnig, G. A. C. Jones, C. G. Smith, G. A. D. Briggs, and M. R. Buitelaar, Phys. Rev. Lett. **106**, 206801 (2011).
[13] G. Giavaras, unpublished

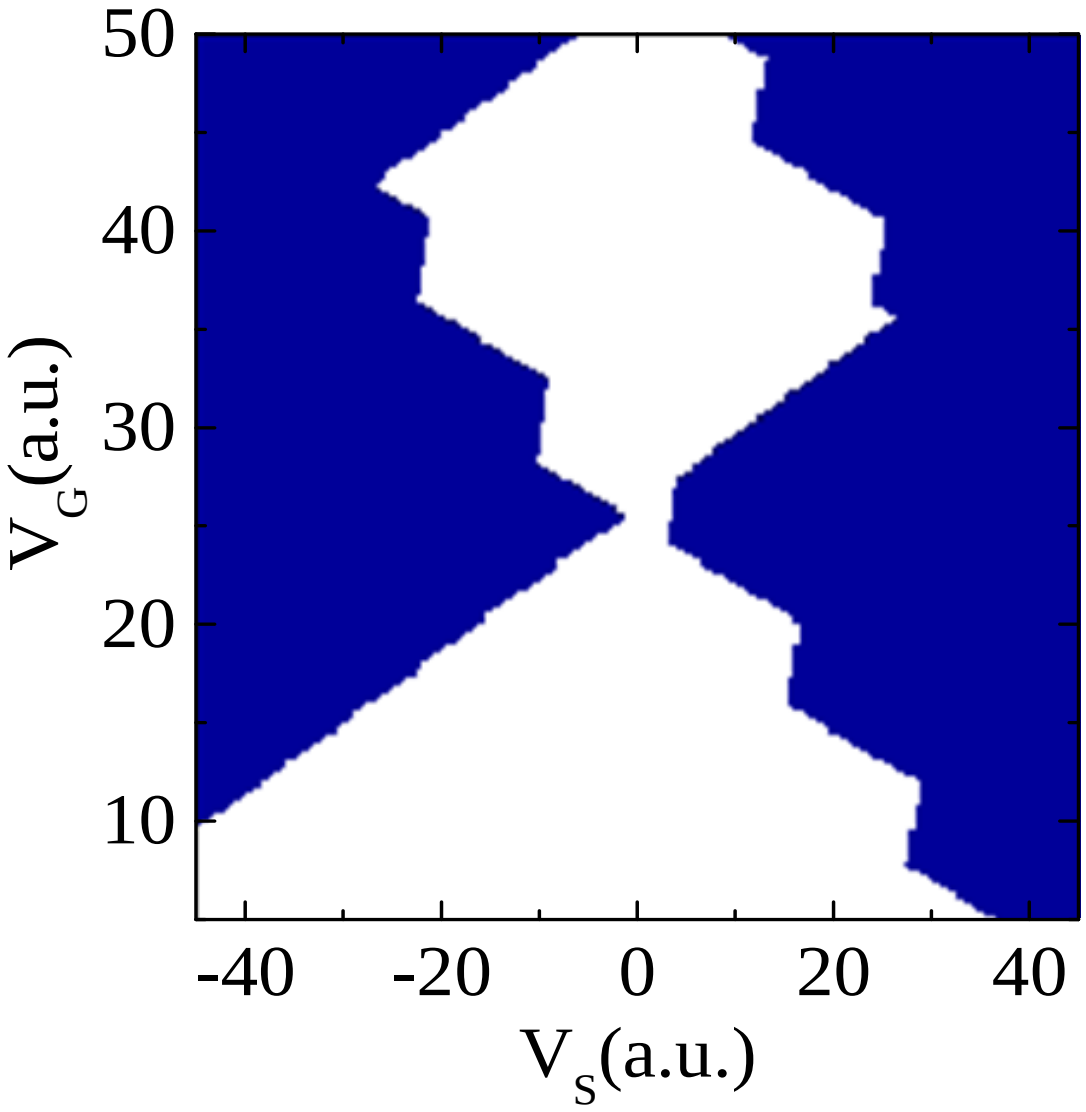

FIG. 1: Coulomb diamond structure for a double quantum dot calculated by the constant charging model. The white region corresponds to the Coulomb blockade region. The parameters (a.u.) are: $E_{C1} = 5$, $E_{C2} = 25$, $E_{C12} = 0.2$, $E_{\rm off} = -0.25$, $C_1 = 1.1$, $C_2 = 1.0$, $D_1 = 0.33$, $D_2 = 0.66$.

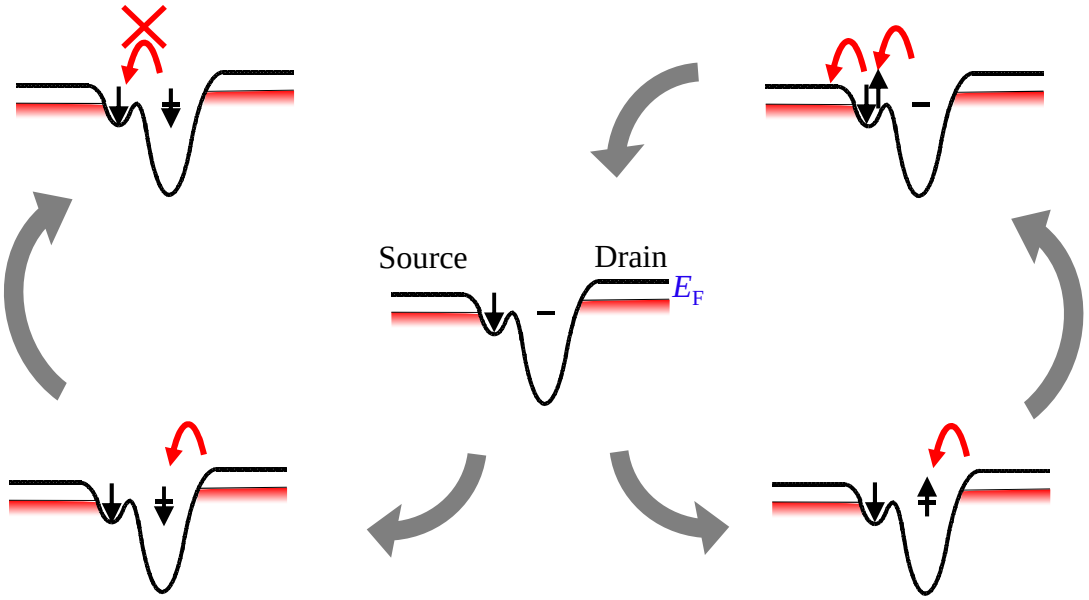

FIG. 2: Schematic representation of the transport cycle in the spin blockade regime. If a state in the bias window has no double occupation on the left dot the current is blocked. The spin-orbit interaction and the microwave field can lift the spin blockade by inducing singlet-triplet transitions.

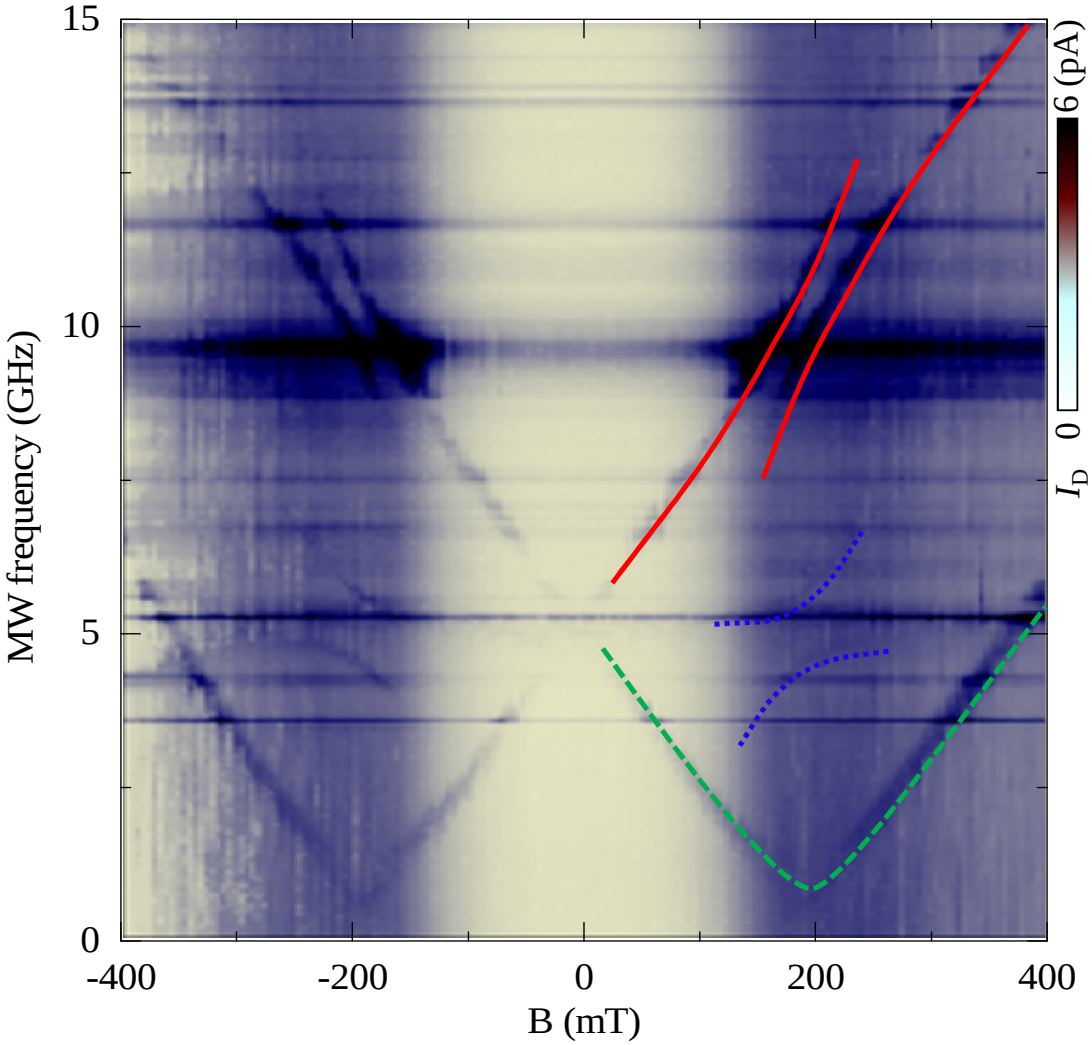

FIG. 3: Intensity plot of leakage current I_D. For $B > 0$ the high-current EDSR curves due to the transitions T_-–S (red solid), T_0–S (blue dotted), T_+–S (green dashed) are indicated.

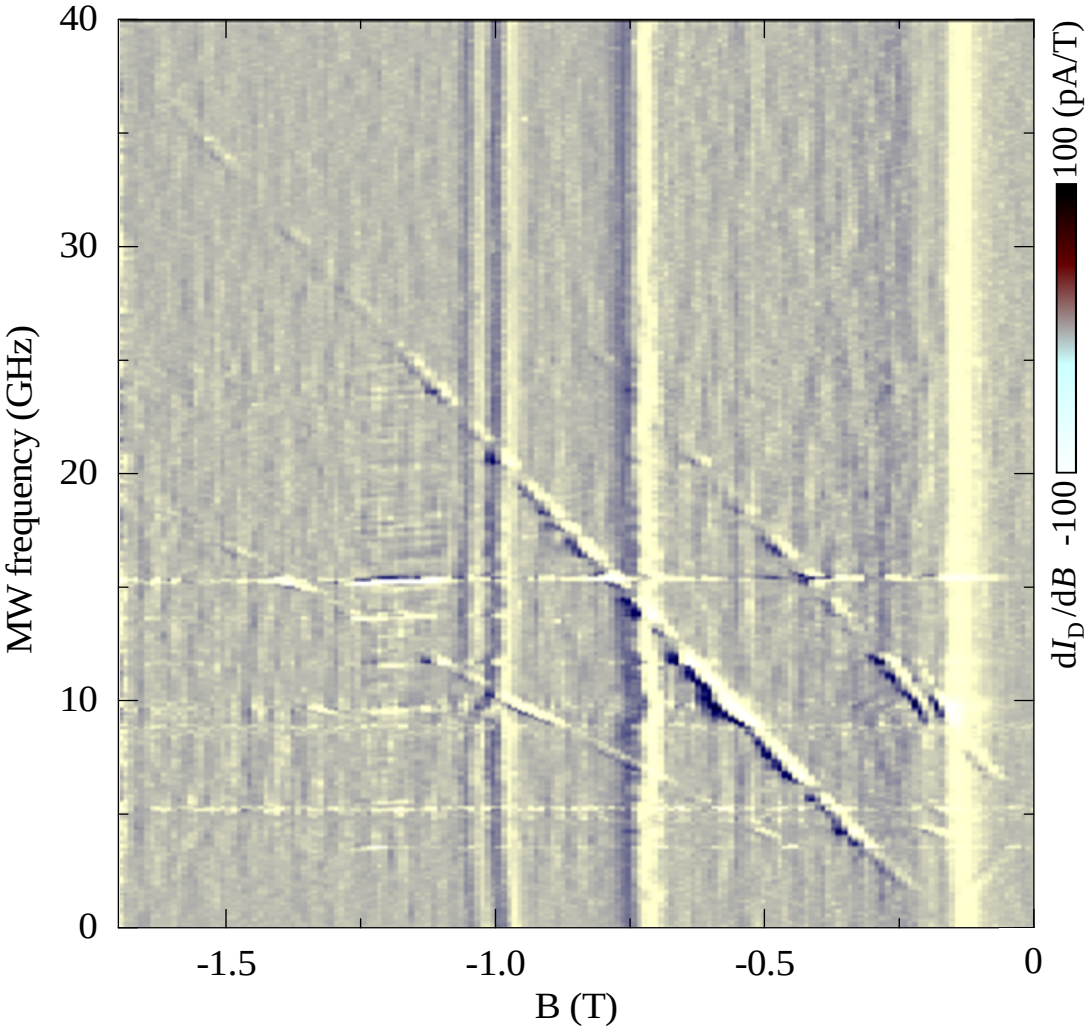

FIG. 4: Intensity plot of dI_D/dB at high microwave frequency and magnetic field.

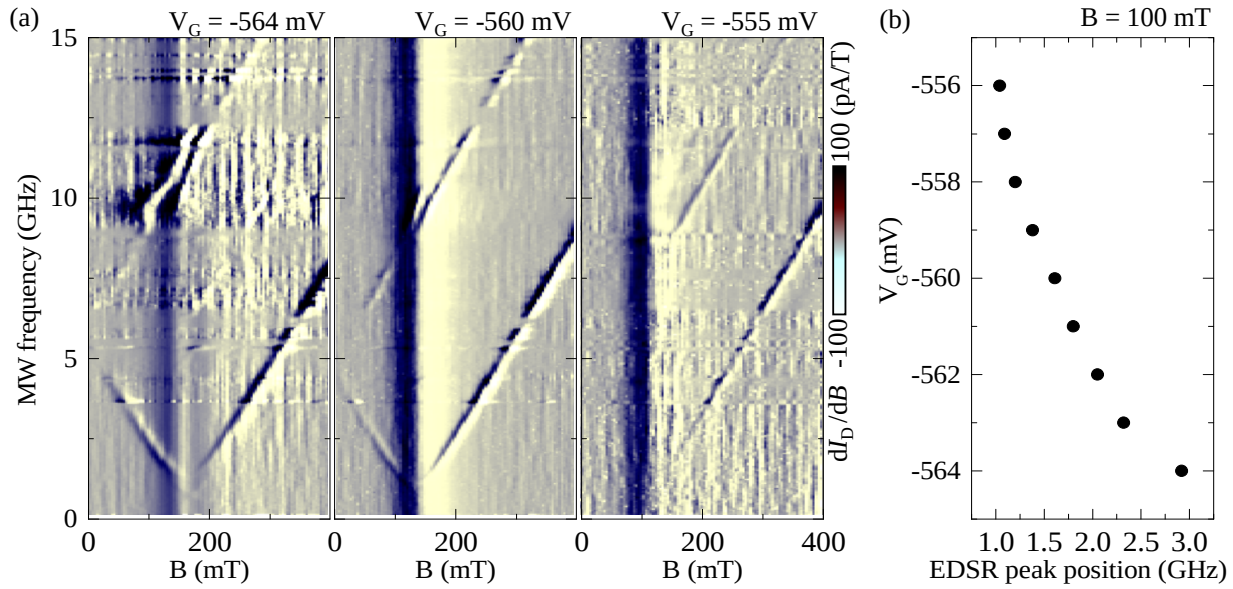

FIG. 5: (a) Intensity plot of dI_D/dB for three different values of the gate voltage V_G. (b) Gate voltage dependence of the EDSR peak position for $B = 100$ mT.

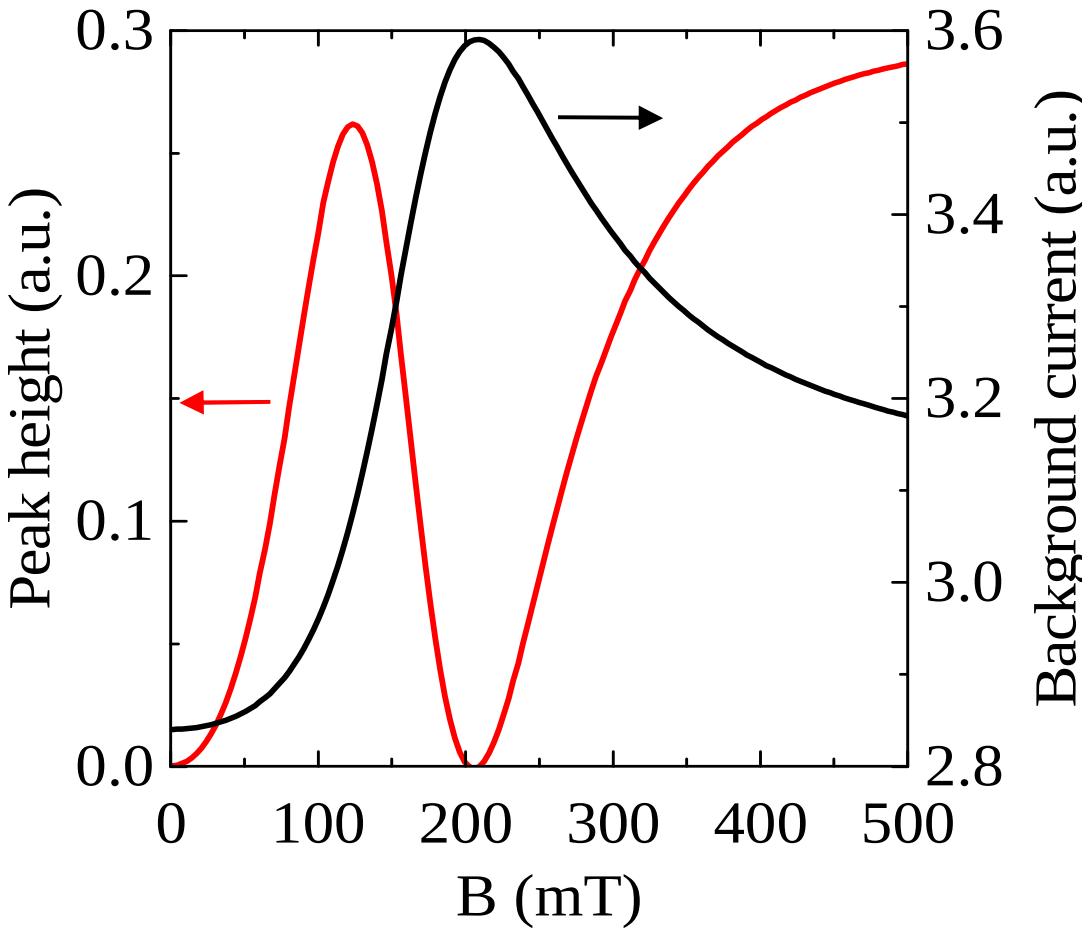

FIG. 6: Peak height (bright line, left axis) for a microwave amplitude $A = 30$ μeV, and background current without the microwave field (dark line, right axis) as a function of the magnetic field near the T_+–S anti-crossing point. The results are derived using the Floquet model described in the supplemental material. See also Figs. 2(c) and (d) in the main article.